Uplink cellular network models with Ginibre deployed base stations

Takuya Kobayashi
Tokyo Institute of Technology
Japan

Naoto Miyoshi
Tokyo Institute of Technology
Japan

***Abstract*—Stochastic geometry models have been attracting attention as tractable models of wireless communication networks. Most prior studies on such models assume that the wireless nodes are placed according to homogeneous Poisson point processes (PPPs); that is, their spatial correlation is ignored. Recently, a stochastic geometry model of downlink cellular networks was proposed in which the wireless base stations (BSs) are deployed according to the Ginibre point process (GPP). The GPP can express repulsion between BSs. On the other hand, the uplink analysis is more complicated than the downlink one since the transmit power of each mobile user depends on its location. In this study, we propose two approximation models for uplink cellular networks in which BSs are deployed according to the GPP. For these models, we derive computable representations for two performance indices and investigate the impact of varying the power control parameter on the network performance.**

I. Introduction

Stochastic geometry models, whose analyses are based on the theory of point processes and stochastic geometry [1], [2], have been attracting attention as tractable models of wireless communication networks. Most prior studies on such stochastic geometry models assume that the wireless nodes (base stations; BSs) are placed according to homogeneous Poisson point processes (PPPs). This means that the wireless nodes are positioned independently of each other and their spatial correlation is ignored. Recently, a stochastic geometry model of cellular networks in which the wireless BSs are deployed according to the Ginibre point process (GPP) was proposed and analyzed with respect to the downlink [3]. The GPP is a determinantal point process, and it accounts for the repulsion between the BSs (see, e.g., [4], [5] for a description of the GPP and general determinantal point processes). In addition, the downlink network model in which the BSs are deployed according to the α-Ginibre point processes (α-GPPs), which constitute an intermediate class between the PPP and GPP, was analyzed [6] and a study of fitting the α-GPP to actual BS deployments was also performed [7].

On the other hand, the analysis of the uplink is more complicated than that of the downlink since, due to the fractional power control (FPC), the transmit power of the mobile user equipment (UE) depends on its location. Therefore, the uplink analsis requires a different approach from the downlink one, and we can consider two scenarios; a UE-centric scenario and a BS-centric one. That is, we first determine the deployments of UEs (resp. BSs) using a point process, and then determine the deployments of BSs (resp. UEs) in another way. Novlan *et al.* [8] proposed a model wherein the locations of the UEs follow a PPP and the communication distances of the UEs from their associated BSs follow an independent identical distribution. Furthermore, the model proposed in [9] places the UEs in annular areas around a typical BS. The model of [8] is regarded as that following the UE-centric scenario, and the model of [9] is following the BS-centric one.

In this study, we propose two distinct approximation models for the analysis of uplink cellular networks in which BSs are deployed according to the GPP. One is BS-centric and the other is UE-centric. For these models, we derive numerically computable representations for the coverage probability, i.e., a complementary cumulative distribution function (CCDF) of the uplink signal-to-interference-plus-noise-ratio (SINR), and the average rate; then we investigate the impact of the optimal power control parameter on these performance indices. By taking the correlation of BS deployments into account, we expect that the models will enable more accurate analyses to be conducted.

The rest of this paper is organized as follows. In the next section, we describe our stochastic geometry model of uplink cellular networks and derive general formulae for the performance indices, i.e., the coverage probability and average rate. In Section III, we propose two different approximation models wherein the BSs are deployed according to the GPP, and we also derive numerically computable representations of coverage probability for the respective models. The results of numerical experiments are described in Section IV, and concluding remarks are given in Section V. The Appendix A is a brief review of the GPP; we give its definition and some useful properties as well as provide a scaled version and the Palm version of the process.

II. Stochastic geometry model of uplink cellular networks

Here, we describe the stochastic geometry model of the uplink of a cellular LTE network and derive basic formulae for performance indices.

A. Model description

There is no intra-cell interference in SC-FDMA on the uplink. Thus, we suppose that each BS selects only one active UE uniformly from the cell area of the BS itself. Let Φ_{B} denote a point process on $\mathbb{R}^2$, and let X_i, $i \in \mathbb{N} \cup \{0\}$, denote the points of Φ_{B}. The point process Φ_{B} represents the configuration of the BSs, and we refer to the BS located at X_i as BS i. In the same way, let Φ_{U} denote a point process on $\mathbb{R}^2$ and let Y_i, $i \in \mathbb{N} \cup \{0\}$, denote the points of Φ_{U}. The point

978-0-9836283-9-2

process $\Phi_{\rm U}$ represents the configuration of active UEs, and we refer to the UE located at Y_i as UE i. We assume that UE i is connected to BS i, $i \in \mathbb{N} \cup \{0\}$. Assuming that there is only one active UE in each cell, $\Phi_{\rm B}$ and $\Phi_{\rm U}$ have the same intensity λ. The path-loss function ℓ representing the attenuation of the signal with distance is given by $\ell(r) = K\, r^{-\beta}$, $r > 0$, where $K > 0$ is the path-loss coefficient and $\beta > 2$ is the path-loss exponent.

Assuming the homogeneity of the transmitted signals and the locations of UEs, we can, without loss of generality, put a typical BS at the origin $o = (0, 0)$. Furthermore, we assume that the point process $\Phi_{\rm U}$ and $\Phi_{\rm B}$ are simple (the probability that there are more than one point in the same place is 0), locally finite a.s. and also stationary. We also assume that Rayleigh fading describes the random effect of fading from UE i to the typical BS at the origin and denote it by h_i; that is, the h_i, $i \in \mathbb{N} \cup \{0\}$, are mutually independent and exponentially distributed with unit mean and are independent of the point processes $\Phi_{\rm U}$ and $\Phi_{\rm B}$. In the setting described above, the signal power $p_{i,0}$ received at the origin from UE i is given by

$$p_{i,0} = p_i\, h_i\, \ell(|Y_i|), \tag{1}$$

where p_i denotes the transmit power emitted by UE i. The SINR of the BS from the associated UE is represented as

$$\mathrm{SINR}_o = \frac{p_{0,0}}{W_o + I_o}, \tag{2}$$

where I_o denotes the cumulative interference received by the BS at the origin (i.e. $X_0 = o$), and W_o denotes a random variable representing the thermal noise at the origin. The cumulative interference I_o is expressed as

$$I_o = \sum_{j \in \mathbb{N}} p_{j,0}.$$

W_0 is independent of $\Phi_{{\rm U},h} = \{(Y_i, h_i)\}_{i \in \mathbb{N} \cup \{0\}}$ and $\Phi_{\rm B}$, and we assume that the Laplace-Stieltjes transform (LST) of W_o is computable.

On the physical uplink data shared channel (PUSCH), the transmit power emitted by a UE is generally influenced by the number of Radio Blocks allocated to it, a corrective factor depending on the Transport Format, and the closed loop command issued by the associated BS (see [10] for details). However, in order to analyze the effect of the compensation factor ϵ, we here consider a simplified case in which the transmit power p_i is given in terms of mW as

$$p_i = \frac{p}{(\ell(R_i))^\epsilon}, \tag{3}$$

where p denotes the target received signal power at each BS and $R_i = |X_i - Y_i|$ denotes the communication distance between BS i and UE i. In (3), if $\epsilon = 0$, all the UEs emit the same power p, while if $\epsilon = 1$, the pathloss is completely inverted by the power control. Applying (3) to (1), the received power $p_{i,0}$ becomes

$$p_{i,0} = \begin{cases} p\, h_0\, (\ell(R_0))^{1-\epsilon}, & i = 0, \\ p\, h_i\, \ell(|Y_i|)\, (\ell(R_i))^{-\epsilon}, & i \neq 0. \end{cases}$$

In the same way, the SINR (2) can be rewritten as

$$\mathrm{SINR}_o = \frac{p\, h_0\, (\ell(|Y_0|))^{1-\epsilon}}{W_o + \sum_{j=1}^{\infty} p\, h_j\, \ell(|Y_j|)(\ell(R_j))^{-\epsilon}}. \tag{4}$$

B. Performance indices

We will take the coverage probability and the average rate to be the performance indices. The coverage probability is defined as $p_c(\theta, \beta, \epsilon) = \mathbf{P}_{\rm B}^o\,(\mathrm{SINR}_o > \theta)$; that is, the probability that the SINR of the typical BS achieves a predefined SINR threshold $\theta > 0$, where $\mathbf{P}_{\rm B}^o\,(\cdot)$ denotes the Palm probability associated with $\Phi_{\rm B}$. The following general formula will be used later, by giving it specific distributions of $\{|Y_j|\}_{j \in \mathbb{N} \cup \{0\}}$ and $\{R_j\}_{j \in \mathbb{N}}$.

Lemma 1: For the uplink cellular network model described above, the coverage probability is given by

$$p_c(\theta, \beta, \epsilon) = \mathbf{E}_{\rm B}^o \left[\mathcal{L}_W(\xi) \prod_{j \in \mathbb{N}} \left(1 + \theta \left(\frac{{R_j}^\epsilon |Y_0|^{1-\epsilon}}{|Y_j|} \right)^\beta \right)^{-1} \right], \tag{5}$$

where $\xi = (\theta/p)\, (|Y_0|^\beta / K)^{1-\epsilon}$ and $\mathcal{L}_W$ denotes the LST of W_o.

Proof: From (4), we have

$$\begin{aligned} \mathbf{P}_{\rm B}^o\,(\mathrm{SINR}_0 > \theta) &= \mathbf{P}_{\rm B}^0 \left(\frac{p\, h_0\, (\ell(|Y_0|))^{1-\epsilon}}{W_o + I_o} > \theta \right) \\ &= \mathbf{P}_{\rm B}^o \left(h_0 > \frac{\theta\, (W_o + I_o)}{p\, (\ell(|Y_0|))^{1-\epsilon}} \right). \end{aligned}$$

Since h_0 is exponentially distributed with unit mean, and W_o and I_o are mutually independent, we have

$$\begin{aligned} &\mathbf{P}_{\rm B}^o \left(h_0 > \frac{\theta\, (W_o + I_o)}{p\, (\ell(|Y_0|))^{1-\epsilon}} \right) \\ &= \mathbf{E}_{\rm B}^o \left[\exp\left(-\frac{\theta\, (W_o + I_o)}{p\, (\ell(|Y_0|))^{1-\epsilon}} \right) \right] \\ &= \mathbf{E}_{\rm B}^o \left[e^{-\theta W_o / p(\ell(|Y_0|))^{1-\epsilon}}\, e^{-\theta I_o / p(\ell(|Y_0|))^{1-\epsilon}} \right] \\ &= \mathbf{E}_{\rm B}^o \left[\mathcal{L}_W(\xi)\, \mathbf{E} \left[e^{-\xi I_o} \middle| \Phi_{\rm U}, \{R_i\}_{i \in \mathbb{N}} \right] \right]. \end{aligned} \tag{6}$$

Furthermore, since h_j, $j \in \mathbb{N}$, are mutually independent, we have

$$\begin{aligned} &\mathbf{E} \left[e^{-\xi I_o} \middle| \Phi_{\rm U}, \{R_i\}_{i \in \mathbb{N}} \right] \\ &= \prod_{j \in \mathbb{N}} \mathbf{E} \left[e^{-\theta h_j \ell(|Y_j|)(\ell(R_j))^{-\epsilon} / (\ell(|Y_0|))^{1-\epsilon}} \middle| \Phi_{\rm U}, \{R_i\}_{i \in \mathbb{N}} \right] \\ &\overset{(a)}{=} \prod_{j \in \mathbb{N}} \left(1 + \frac{\theta\, \ell(|Y_j|)}{(\ell(R_j))^\epsilon\, (\ell(|Y_0|))^{1-\epsilon}} \right)^{-1} \\ &\overset{(b)}{=} \prod_{j \in \mathbb{N}} \left(1 + \theta \left(\frac{{R_j}^\epsilon\, |Y_0|^{1-\epsilon}}{|Y_j|} \right)^\beta \right)^{-1}, \end{aligned} \tag{7}$$

where (a) follows from the LST $\mathcal{L}_h(s) = (1+s)^{-1}$ of h_j and (b) follows from $\ell(r) = K\, r^{-\beta}$, $r > 0$. Therefore, applying (7) to (6), we obtain (5). ■

From Lemma 1, we can see that, if $W_o = 0$, the coverage probability is determined by the values of θ, β and ϵ, but does not depend on the values of λ, p and K.

Moreover, the average rate based upon the Shannon capacity formula is defined as $\tau(\beta, \epsilon) = \mathbf{E}_{\rm B}^o\,[\ln(1 + \mathrm{SINR}_o)]$. Since

$\ln(1+\mathrm{SINR}_o) > 0$ a.s., the average rate is expressed using the coverage probability p_c as

$$\begin{aligned}\tau(\beta,\epsilon) &= \int_0^\infty \mathbf{P}_{\mathrm{B}}^o\left(\ln\left(1+\mathrm{SINR}_0\right) > t\right)\mathrm{d}t \\ &= \int_0^\infty \mathbf{P}_{\mathrm{B}}^o\left(\mathrm{SINR}_0 > e^t-1\right)\mathrm{d}t \\ &= \int_0^\infty p_c(e^t-1,\beta,\epsilon)\,\mathrm{d}t.\end{aligned}$$

III. Approximation models

Here, we propose two distinct approximation models for the uplink cellular network described in Section II-A such that the BSs are deployed according to the GPP. We then derive numerically computable integrable representations for the respective models. We assume that a UE connects to the closest BS and that each BS has an active uplink UE. In this paper, we use slash "/" for a BS-centric model such as GPP/Uniform and backslash "\" for a UE-centric one such as PPP\MoSE.

A. Model 1 (GPP/Uniform)

Let us assume that the BS configuration Φ_{B} corresponds to the GPP with intensity λ. It is natural to think that an active UE is uniformly distributed in the Voronoi cell of the associated BS. However, we suppose that the active UE is uniformly distributed in a circle of radius $1/\sqrt{\pi\,\lambda}$ centered at the associated BS independently of others in this model. Due to the homogeneity of the GPP and the i.i.d. arrangement of UEs to the respective associated BSs, the UE locations Φ_{U} are also homogeneous. For this model, we have the following.

Theorem 1 (Coverage probability for GPP/Uniform): The uplink coverage probability for Model 1 is given by

$$\begin{aligned}&p_c(\theta,\beta,\epsilon)\\ &= \int_0^1 \mathcal{L}_W(\xi(v))\prod_{j=1}^\infty \int_0^\infty \frac{x^j e^{-x}}{j!}\,g(v,x)\,\mathrm{d}x\,\mathrm{d}v, \qquad (8)\end{aligned}$$

where $\xi(v) = \theta/(p\,K^{1-\epsilon})\,(v/(\pi\,\lambda))^{\beta(1-\epsilon)/2}$ and g is given by

$$g(v,x) = \frac{1}{2\,\pi}\int_0^1\int_0^{2\pi}\left(1+\theta\left(\frac{v^{1-\epsilon}\,u^\epsilon}{x+u-2\sqrt{u\,x}\,\cos\gamma}\right)^{\beta/2}\right)^{-1}\mathrm{d}\gamma\,\mathrm{d}u.$$

Proof: Let γ_i denote the angle $\angle X_0X_iY_i$. Then, using R_i, X_i, and γ_i, the distance $|Y_i|$ between UE i and the origin is computed as follows.

$$|Y_i|^2 = |X_i|^2 + {R_i}^2 - 2\,|X_i|\,R_i\,\cos\gamma_i. \qquad (9)$$

Since $|Y_j|$ can be expressed as above, we have

$$\begin{aligned}&\left(\frac{{R_j}^\epsilon\,|Y_0|^{1-\epsilon}}{|Y_j|}\right)^\beta\\ &= \left(\frac{{R_j}^{2\epsilon}\,|Y_0|^{2(1-\epsilon)}}{|X_j|^2+{R_j}^2-2\,|X_j|\,R_j\,\cos\gamma_j}\right)^{\beta/2}. \qquad (10)\end{aligned}$$

From Proposition 3 in Appendix A, we can consider $|X_i|$, $i\in\mathbb{N}$, mutually independent, and so are $|Y_i|$, $i\in\mathbb{N}\cup\{0\}$ from (9) since $\{|X_i|\}_{i\in\mathbb{N}}$, $\{R_i\}_{i\in\mathbb{N}}$ and $\{\gamma_i\}_{i\in\mathbb{N}}$ are independent. Thus, applying (10) to (5) of Lemma 1 and applying Proposition 3 in Appendix A again, we obtain

$$\begin{aligned}&\mathbf{E}_{\mathrm{B}}^o\left[\prod_{j\in\mathbb{N}}\left(1+\theta\left(\frac{{R_j}^\epsilon\,|Y_0|^{1-\epsilon}}{|Y_j|}\right)^\beta\right)^{-1}\middle|\,Y_0\right]\\ &= \prod_{j\in\mathbb{N}}\mathbf{E}_{\mathrm{B}}^o\left[\left(1+\theta\left(\frac{{R_j}^\epsilon\,|Y_0|^{1-\epsilon}}{|Y_j|}\right)^\beta\right)^{-1}\middle|\,Y_0\right]\\ &= \prod_{j=1}^\infty\int_{x=0}^\infty \frac{x^j e^{-x}}{j!}\,g(\pi\,\lambda\,|Y_0|^2,x)\,\mathrm{d}x. \qquad (11)\end{aligned}$$

Hence, we obtain (8) by applying (11) to (5) and then integrating with respect to the distribution of $|Y_0|$. ■

B. Model 2 (PPP\MoSE)

This model follows the similar idea to that in [8]. In this model, we suppose that the UE configuration Φ_{U} forms a realization of a PPP with intensity λ, while the distribution of $\{R_j\}_{j\in\mathbb{N}\cup\{0\}}$ is determined as follows. Although R_j, $j\in\mathbb{N}\cup\{0\}$, are primarily not independent because of their dependence on the BS configuration, we suppose that they are mutually independent. Now, we focus on a fixed UE i. If the BS configuration Φ_{B} corresponds to the GPP with intensity λ independently of Y_i, from Proposition 2 in Appendix A and the remark thereafter, the set of distances from the UE i to all BSs $\{|Y_i-X_j|\}_{j\in\mathbb{N}\cup\{0\}}$ has the same distribution as $\{\sqrt{Z_{i,j}}\}_{j\in\mathbb{N}}$, where $Z_{i,j}$, $j\in\mathbb{N}$, are mutually independent and each $Z_{i,j}$ follows the jth Erlang distribution with a rate parameter $\pi\,\lambda$; i.e. $Z_{i,j}\sim\mathrm{Gam}(j,\pi\,\lambda)$. Thus, since the UE connects to the closest BS, the distance R_i between the UE i and BS i fulfills

$$R_i =_d \min_{j\in\mathbb{N}}\sqrt{Z_{i,j}}. \qquad (12)$$

We refer to the distribution of R_i given by (12) as the MoSE (Minimum of Square-rooted Erlangs) distribution with a parameter $\pi\,\lambda$. The cumulative distribution function (CDF) and the probability density function (pdf) of the MoSE distribution is given by the following lemma.

Lemma 2 (CDF and pdf of MoSE distribution): The CDF $F_{\mathrm{MoSE}}(r)$ and pdf $f_{\mathrm{MoSE}}(r)$ of the MoSE distribution with parameter c are respectively given by

$$F_{\mathrm{MoSE}}(r) = 1-M(c\,r^2), \qquad (13)$$

$$f_{\mathrm{MoSE}}(r) = 2\,c\,r\,M(c\,r^2)\,S(cr^2), \qquad (14)$$

where $r>0$, and $M(u)$ and $S(u)$ are given by

$$M(u) = \prod_{j=0}^\infty\left(\sum_{k=0}^j\frac{u^k}{k!}\,e^{-u}\right), \qquad (15)$$

$$S(u) = \sum_{i=0}^\infty\frac{u^i}{i!}\left(\sum_{k=0}^i\frac{u^k}{k!}\right)^{-1}. \qquad (16)$$

Proof: Let R denote a random variable obeying a MoSE distribution with parameter c. Then, R can be expressed as

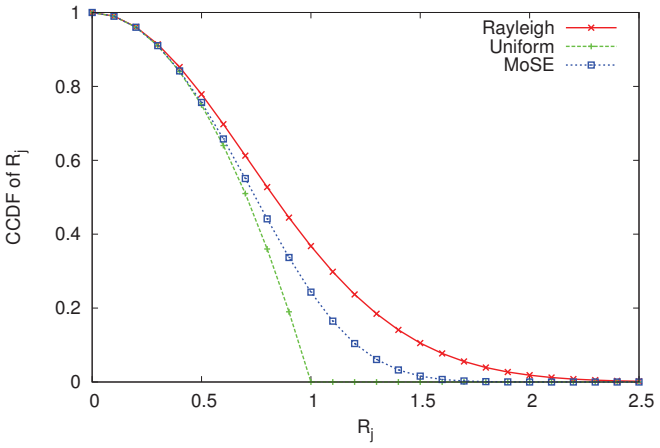

Fig. 1. Comparison of the CCDFs of R_j in the cases of MoSE distribution with parameter 1 ($\overline{F}(r) = 1 - F_{\mathrm{MoSE}}(r)$), Rayleigh ($\overline{F}(r) = \mathrm{e}^{-r^2}$), and Uniform ($\overline{F}(r) = 1 - r^2$, $0 \le r \le 1$).

$R = \min_{j\in\mathbb{N}} \sqrt{Z_j}$, where the $Z_j \sim \mathrm{Gam}(j, c)$, $j \in \mathbb{N}$, are mutually independent. Here, the CDF and pdf of Z_j are respectively given by

$$F_j(x) = 1 - \sum_{k=0}^{j-1} \frac{(cx)^k}{k!} e^{-cx},$$
$$f_j(x) = \frac{c^j x^{j-1}}{(j-1)!} e^{-cx}.$$

Thus, the CDF of R is expressed as

$$\begin{aligned} F_{\mathrm{MoSE}}(r) &= 1 - \mathbf{P}\left(\min_{j\in\mathbb{N}} \sqrt{Z_j} > r\right) \\ &= 1 - \prod_{j=1}^{\infty} \mathbf{P}\left(Z_j > r^2\right) \\ &= 1 - \prod_{j=1}^{\infty} \left(1 - F_j(r^2)\right). \end{aligned}$$

On the other hand, the pdf of R is written by using $f_j(r)$ and $F_j(r)$:

$$f_{\mathrm{MoSE}}(r) = \sum_{i=1}^{\infty} \left(\frac{2\,r\,f_i(r^2)}{1 - F_i(r^2)}\right) \prod_{j=1}^{\infty} \left(1 - F_j(r^2)\right).$$

Taking $M(u)$ and $S(u)$ as (15) and (16) respectively, we obtain $F_{\mathrm{MoSE}}(r)$ and $f_{\mathrm{MoSE}}(r)$ as in (13) and (14) respectively. ■

Instead of the MoSE distribution, if we take the distribution of R_i to be as follows, the model reduces to the PPP\Rayleigh or PPP\Uniform proposed in [8].

- PPP\Rayleigh:

$$\mathbf{P}\left(R_i > r\right) = \mathrm{e}^{-\pi\lambda r^2}. \tag{17}$$

This idea is based on the fact that the distribution of the distance from the origin to the closest point of the PPP follows a Rayleigh distribution.

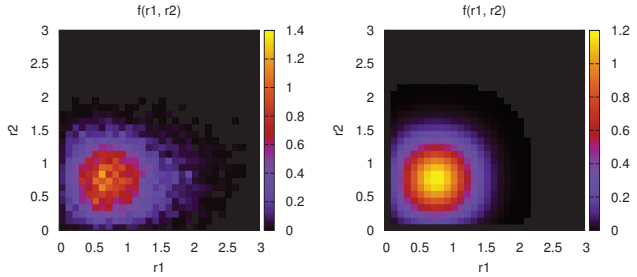

Fig. 2. Top view of the joint density of R_1 and R_2 for the GPP-Simulation model (left) and that under the independence assumption (right). R_1 and R_2 are the distances of the UEs to their respective BSs in two neighboring Voronoi cells.

- PPP\Uniform:

$$\mathbf{P}\left(R_i > r\right) = \begin{cases} 1 - \pi\,\lambda\,r^2 & 0 \le r \le (\pi\,\lambda)^{-1/2}, \\ 0 & r > (\pi\,\lambda)^{-1/2}. \end{cases} \tag{18}$$

Figure 1 compares the CCDFs of R_j in the cases of MoSE, Rayleigh, and Uniform distributions. Compared with the results of [8], we can see that the MoSE distribution is close to the distribution of R_j made from the data of actual BS deployments. Furthermore, we numerically compute the joint pdf $f_{R_1,R_2}(r_1, r_2)$ for the GPP-Simulation model and compare it with the joint pdf of two independent MoSE variables in Fig 2, where the GPP-Simulation model represents the simulation results for the model wherein the BSs are deployed according to the GPP and the UEs are distributed uniformly in the respective Voronoi cells of the associated BSs, and R_1 and R_2 denote the distances of the UEs to their respective associated BSs in two neighboring Voronoi cells. From Fig 2, we can find that the two joint densities are very similar and the independence assumption is appropriate enough.

The following proposition shows that the uplink coverage probability for the PPP\MoSE model can be expressed in a form similar to that for the prior models, i.e., PPP\Rayleigh and PPP\Uniform in [8] .

Proposition 1 ([8]): The uplink coverage probability for PPP\Rayleigh and PPP\Uniform is given by

$$p_c(\theta, \beta, \epsilon) = \int_0^{\infty} \mathcal{L}_W(\xi(v))\, \mathrm{e}^{-v - \int_v^{\infty} H(v,w)\mathrm{d}w}\, \mathrm{d}v, \tag{19}$$

where $\xi(v) = \theta/(pK^{1-\epsilon})\,(v/(\pi\,\lambda))^{\beta(1-\epsilon)/2}$, and H is replaced with H_{R} in the case of PPP\Rayleigh and H_{U} in the case of PPP\Uniform:

$$H_{\mathrm{R}}(v, w) = \int_0^{\infty} e^{-u} \left(1 + \frac{1}{\theta}\left(\frac{w}{v^{1-\epsilon}\,u^{\epsilon}}\right)^{\beta/2}\right)^{-1} \mathrm{d}u,$$
$$H_{\mathrm{U}}(v, w) = \int_0^{1} \left(1 + \frac{1}{\theta}\left(\frac{w}{v^{1-\epsilon}\,u^{\epsilon}}\right)^{\beta/2}\right)^{-1} \mathrm{d}u.$$

The uplink coverage probability for the PPP\MoSE model is given by the following Theorem.

Theorem 2 (Uplink coverage probability for PPP\MoSE): The uplink coverage probability for the PPP\MoSE model is

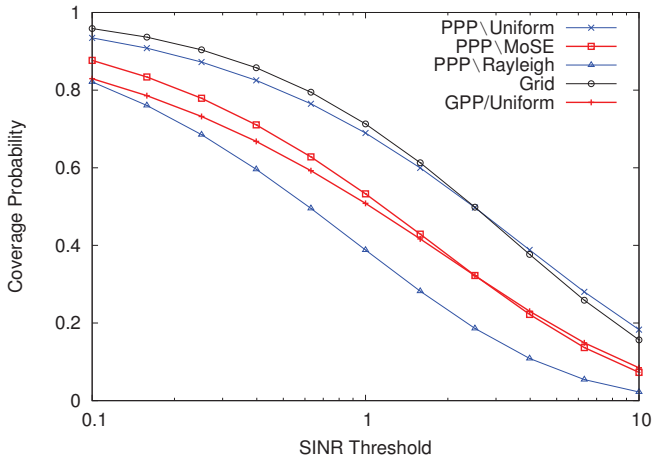

Fig. 3. Comparison of coverage probabilities for PPP\Rayleigh, PPP\Uniform, PPP\MoSE, GPP/Uniform and Grid model with $\beta = 4$ and $\epsilon = 1$.

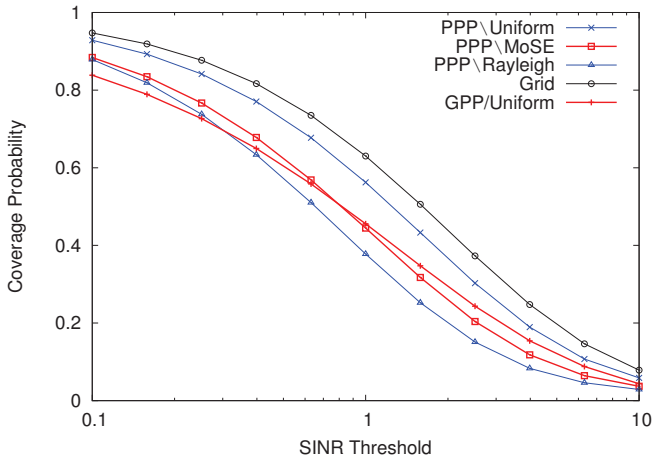

Fig. 4. Comparison of coverage probabilities for PPP\Rayleigh, PPP\Uniform, PPP\MoSE, GPP/Uniform, and Grid model with $\beta = 3.25$ and $\epsilon = 0.75$.

given by replacing $H(v, w)$ in (19) with

$$H_{\mathrm{M}}(v, w) = \int_0^\infty M(u)\, S(u) \left(1 + \frac{1}{\theta} \left(\frac{w}{v^{1-\epsilon}\, u^{\epsilon}}\right)^{\beta/2}\right)^{-1} \mathrm{d}u, \quad (20)$$

where $M(u)$ and $S(u)$ are given by (15) and (16).

Proof: The proof is similar to what is presented in [8]. The difference is that (17) or (18) is replaced with (13) in Lemma 2. That is, the coverage probability is given by (19) in Proposition 1 with

$$H(v, w) = \mathbf{E}\left[\left(1 + \frac{1}{\theta} \left(\frac{w}{v^{1-\epsilon}\, (\pi\, \lambda\, {R_j}^2)^{\epsilon}}\right)^{\beta/2}\right)^{-1}\right]. \quad (21)$$

Here, (20) is obtained by applying (13) in Lemma 2 to (21). ■

IV. Numerical Experiments

Here, we show the results of numerical experiments on computing the coverage probabilities and the average rates. For simplicity, we assumed the thermal noise W_o to be 0.

A. Coverage probability

Figures 3 and 4 show the coverage probabilities for given values of the SINR threshold θ in five models: GPP/Uniform, PPP\MoSE, PPP\Rayleigh, PPP\Uniform and Grid with the pair of path-loss exponent β and compensation factor ϵ given as $(\beta, \epsilon) = (4, 1)$ and $(3.25, 0.75)$. Note that this Grid model is one in which the BSs are deployed on hexagonal grids and the UEs are uniformly distributed one to each cell, and its coverage probability was evaluated via Monte-Carlo simulation due to its intractability. Comparing Fig. 3 with Fig. 5 in [8], we can see that the coverage probabilities for the two GPP based models are very close to that for the corresponding model made from the data of actual BS deployments.

Figure 5 plots the optimal compensation parameter (the value of ϵ maximizing the coverage probability for a given SINR target θ), denoted by ϵ^*, as a function of the SINR threshold. Here, GPP-Simulation results are for a model in which the BSs are deployed according to the GPP and the UEs are uniformly distributed in the Voronoi cells of the associated BSs. The values of ϵ^* for PPP\MoSE, PPP\Rayleigh and PPP\Uniform show a similar tendency, but become smaller in the order of PPP\Uniform, PPP\MoSE, and PPP\Rayleigh for any SINR threshold. In addition, the results for GPP/Uniform are close to those of GPP-Simulation for a relatively low SINR threshold. Therefore, the GPP/Uniform model is a reasonable approximation of GPP BS deployments. Furthermore, a similar tendency can be seen with Grid and GPP/Uniform. However, ϵ^* increases as the SINR threshold decreases in the cases of GPP/Uniform and GPP-Simulation, while it converges to around 0.38 as $\theta \to 0$ in the case of Grid. This indicates that the optimal compensation parameter ϵ^* varies depending on the deployment of the BSs. In particular, the optimal compensation parameter of GPP-based BS deployment is larger than the optimal one for the Grid deployment.

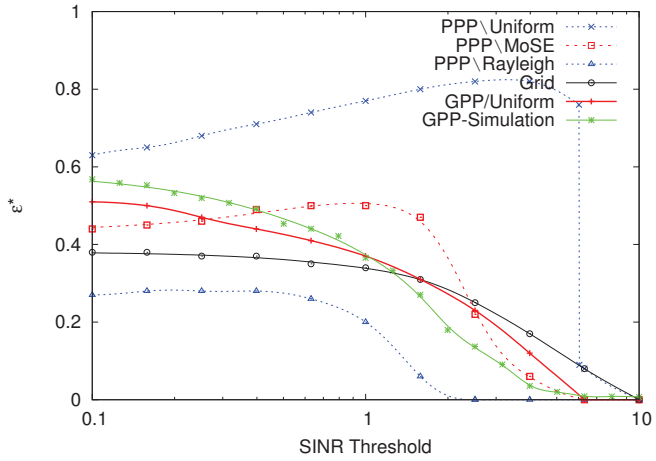

Fig. 5. Plots of the coverage-maximizing ϵ^* for given values of SINR threshold θ and $\beta = 3.75$.

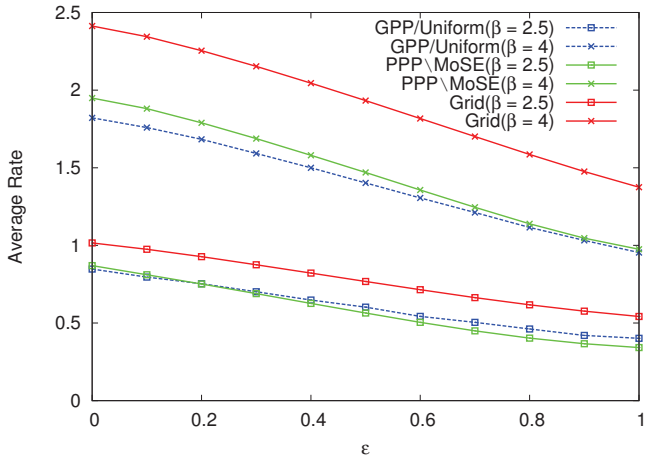

Fig. 6. Average rate τ as a function of the power control parameter ϵ for different path-loss exponents $\beta = 2.5$ and 4.

B. Average rate

Figure 6 plots the average rate τ as a function of ϵ for different path-loss exponents $\beta = 2.5$ and 4, for the GPP/Uniform, PPP\MoSE and Grid models. From Fig. 6, the average rate also increases with β for any ϵ. Furthermore, the average rate is maximized when $\epsilon = 0$ in each model. This is because the interference from outside cells can not be mitigated enough by increasing the transmit power of the cell-edge UEs. In addition, the average rate of the Grid model is larger than that of the GPP/Uniform and PPP\MoSE models. This is because the coverage probability of Grid model is larger than that of the other models. From the definition of average rate, we can see that if the coverage probability is larger for any value of the SINR threshould, the average rate also becomes larger.

V. Conclusion

We proposed two approximation models for analyzing uplink cellular networks. In both models, the BSs are deployed according to the GPP. We derived computable integral representations for the coverage probability and average rate. By comparing the coverage probability with that using data from actual BS deployments reported in [8], we found that the proposed models could represent the irregular configuration of actual BSs. We observed that the optimal compensation parameter ϵ^* increases as the SINR threshold decreases in the GPP/Uniform model, whereas ϵ^* converges to around 0.38 in the Grid model. Furthermore, the results for the GPP/Uniform model were close to those of GPP-Simulation model for relatively low SINR thresholds. If you consider the application to actual networks, you may extend the GPP model to the α-GPP one with fitting the α-GPP to the actual BS deployments [6], [7].

In the future, we plan to do an improvement in computation time. Indeed, the computation time for the proposed models is faster than that for the GPP-Simulation. However, since the representations of the performance indices for the GPP-based models include infinite product, infinite sum and multiple integration, the computation takes longer time than that for the Grid and PPP models. To improve this, the Monte-Carlo sampling of Erlang random variables might be effective. Furthermore, we also plan to do an uplink analysis of a heterogeneous network that consists of BSs of different types and with different cell-range distributions. That is, we will apply cluster point processes or α-GPPs to heterogeneous networks.

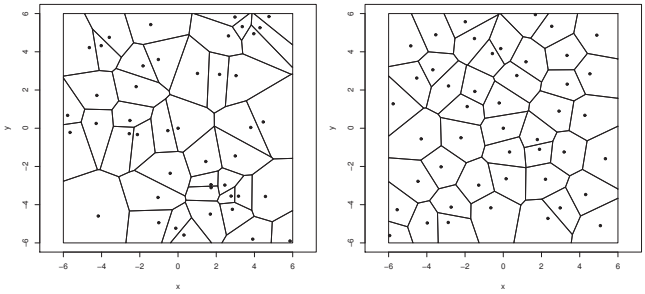

Fig. 7. Voronoi tessellations of samples of a PPP (left) and GPP (right).

Acknowledgments

The second author (NM)'s work was supported by a JSPS (Japan Society for the Promotion of Science) Grant-in-Aid for Scientific Research (C) 25330023.

References

[1] F. Baccelli and B. Błaszczyszyn (2009), "Stochastic geometry and wireless networks, volume I: Theory/volume II: Applications," *Foundations and Trends in Networking*, **3**, 249–449/**4**, 1–312.

[2] M. Haenggi (2012), *Stochastic Geometry for Wireless Networks*, Cambridge University Press.

[3] N. Miyoshi and T. Shirai (2014), "A cellular network model with Ginibre configurated base stations," to appear in *Adv. Appl. Probab.*, **46**.

[4] T. Shirai and Y. Takahashi (2003), "Random point fields associated with certain Fredholm determinants. I. Fermion, Poisson and Boson point processes," *J. Funct. Anal.*, **205**, 414–463.

[5] J. B. Hough, M. Krishnapur, Y. Peres and B. Virág (2009), *Zeros of Gaussian Analytic Functions and Determinantal Point Processes*, Amer. Math. Soc..

[6] I. Nakata and N. Miyoshi (2014), "Spatial stochastic models for analysis of heterogeneous cellular networks with repulsively deployed base stations," to appear in *Performance Evaluation*.

[7] N. Deng, W. Zhou and M. Haenggi (2014), "The ginibre point process as a model for wireless networks with repulsion," arXiv:1401.3677 [cs.IT].

[8] T. D. Novlan, H. S. Dhillon, and J. G. Andrews (2013), "Analytical modeling of uplink cellular networks," *IEEE Trans. on Wireless Comm.*, **12**, 2669–2679.

[9] M. Coupechoux and J. Kelif (2011), "How to set the fractional power control compensation factor in LTE?," *IEEE Sarnoff Symp.*, 1–5.

[10] 3GPP. 36.213 Physical Layer Procedures.

[11] H. S. Dhillon, R. Ganti, F. Baccelli and J. G. Andrews (2012), "Modeling and analysis of K-tier downlink heterogeneous cellular networks," *IEEE J. Select. Areas Comm.*, **30**, 550–560.

[12] A. Goldman (2010), "The Palm measure and the Voronoi tessellation for the Ginibre process," *Ann. Appl. Probab.*, **20**, 90–128.

Appendix

In this section, we define the GPP and describe its tractable properties. The GPP is a determinantal point process on the

complex plane $\mathbb{C}$. Let Φ denote a simple point process on $\mathbb{C}$ and $\rho_n\colon \mathbb{C}^n \to \mathbb{R}_+$, $n \in \mathbb{N}$, denote its joint intensities with respect to some locally finite measure ν on $(\mathbb{C}, \mathcal{B}(\mathbb{C}))$. That is, for any continuous symmetric function f on $\mathbb{C}^n$ with compact support, we have

$$\mathbf{E}\left[\sum_{\substack{X_1,\ldots,X_n\in\Phi\\ \text{distinct}}} f(X_1, X_2, \ldots, X_n)\right] = \int_{\mathbb{C}^n} f(z_1,\ldots,z_n)\rho_n(z_1,\ldots,z_n)\,\nu(\mathrm{d}z_1)\cdots\nu(\mathrm{d}z_n).$$

The point process Φ is said to be a determinantal point process with kernel $K\colon \mathbb{C}^2 \to \mathbb{C}$ with respect to the reference measure ν if the ρ_n, $n \in \mathbb{N}$, satisfy

$$\rho_n(z_1,\ldots,z_n) = \det(K(z_i,z_j))_{1\le i,j\le n},$$

for $z_1,\ldots,z_n \in \mathbb{C}$, where $\det$ denotes the determinant. Furthermore, Φ is said to be the GPP if the kernel K is given by $K(z,w) = \mathrm{e}^{z\overline{w}}$, $z, w \in \mathbb{C}$, with respect to the Gaussian measure $\nu(\mathrm{d}z) = \pi^{-1}\,\mathrm{e}^{-|z|^2}\,m(\mathrm{d}z)$, where $\overline{w}$ denotes the conjugate of $w \in \mathbb{C}$ and m denotes the Lebesgue measure on $(\mathbb{C}, \mathcal{B}(\mathbb{C}))$. This choice of pair of K and ν is not unique. Indeed, the determinantal point process associated with the kernel $\tilde{K}(z,w) = \pi^{-1}\mathrm{e}^{-(|z|^2+|w|^2)/2}\mathrm{e}^{z\overline{w}}$ with respect to $\tilde{\nu}(\mathrm{d}z) = m(\mathrm{d}z)$ coincides with the GPP. From this expression, it is easy to see that $\tilde{\rho}_n(z_1,\ldots,z_n) = \det(\tilde{K}(z_i,z_j))_{1\le i,j\le n}$ is motion-invariant, or equivalently, the GPP is motion-invariant (stationary and isotropic). From its definition, we see that $\mathbf{E}\left[\Phi(C)\right] = m(C)/\pi$ for $C \in \mathcal{B}(\mathbb{C})$; i.e. the (first order) intensity is equal to π^{-1} with respect to the Lebesgue measure. In order to adjust the intensity, we consider a scaled GPP Φ_c with a scaling parameter $c > 0$. Φ_c is given by the kernel $K_c(z,w) = c\,\mathrm{e}^{cz\overline{w}}$ with respect to the reference measure $\nu_c(\mathrm{d}z) = \pi^{-1}\,\mathrm{e}^{-c|z|^2}\,m(\mathrm{d}z)$, or equivalently, $\tilde{K}_c(z,w) = (c/\pi)\,\mathrm{e}^{-c(|z|^2+|w|^2)/2}\,\mathrm{e}^{cz\overline{w}}$ with respect to the Lebesgue measure. Since $\mathbf{E}\left[\Phi_c(C)\right] = (c/\pi)\,m(C)$, Φ_c has the intensity c/π.

One of the useful properties of the GPP comes from its radial symmetry, and it is described as follows.

Proposition 2 (Kostlan): Let X_i, $i \in \mathbb{N}$, denote the points of GPP Φ. Then, the set $\{|X_i|\}_{i\in\mathbb{N}}$ has the same distribution as $\left\{\sqrt{Z_i}\right\}_{i\in\mathbb{N}}$, where the Z_i, $i \in \mathbb{N}$, are mutually independent and each Z_i follows the ith Erlang distribution with a unit rate parameter, denoted by $Z_i \sim \mathrm{Gam}(i,1)$, $i \in \mathbb{N}$.

Proposition 2 can be extended to scaled GPP Φ_c; i.e., for the points X_i, $i \in \mathbb{N}$, of Φ_c, the set $\{|X_i|\}_{i\in\mathbb{N}}$ has the same distribution as $\left\{\sqrt{Z_i}\right\}_{i\in\mathbb{N}}$, where Z_i, $i \in \mathbb{N}$, are mutually independent and each Z_i follows the ith Erlang distribution with rate parameter c, denoted by $Z_i \sim \mathrm{Gam}(i,c)$, $i \in \mathbb{N}$.

Moreover, we can extend Proposition 2 to the Palm version. From [4], [12], the kernel K^o of the reduced Palm version $\Phi^o = (\Phi \mid \Phi(\{o\}) = 1) \setminus \{o\}$ of GPP is given by

$$K^o(z,w) = \pi^{-1}\mathrm{e}^{-(|z|^2+|w|^2)/2}(\mathrm{e}^{z\overline{w}} - 1),$$

with respect to the Lebesgue measure. The following proposition is obtained by applying this kernel to Theorem 4.7.1 in [5].

Proposition 3: Let X_i, $i \in \mathbb{N}$, denote the points of the reduced Palm version Φ^o of GPP. Then, the set $\{|X_i|\}_{i\in\mathbb{N}}$ has the same distribution as $\left\{\sqrt{Z_i}\right\}_{i=2}^{\infty}$, where the Z_i, $i \in \mathbb{N}$, are mutually independent and each $Z_i \sim \mathrm{Gam}(i,1)$, $i \in \mathbb{N}$.